# *4D tomographic reconstruction of the tropospheric wet refractivity using the concept of virtual reference station, case study: northwest of Iran*

**Zohre Adavi & Masoud Mashhadi-Hossainali**

**Meteorology and Atmospheric Physics**

ISSN 0177-7971

Meteorol Atmos Phys
DOI 10.1007/s00703-014-0342-4

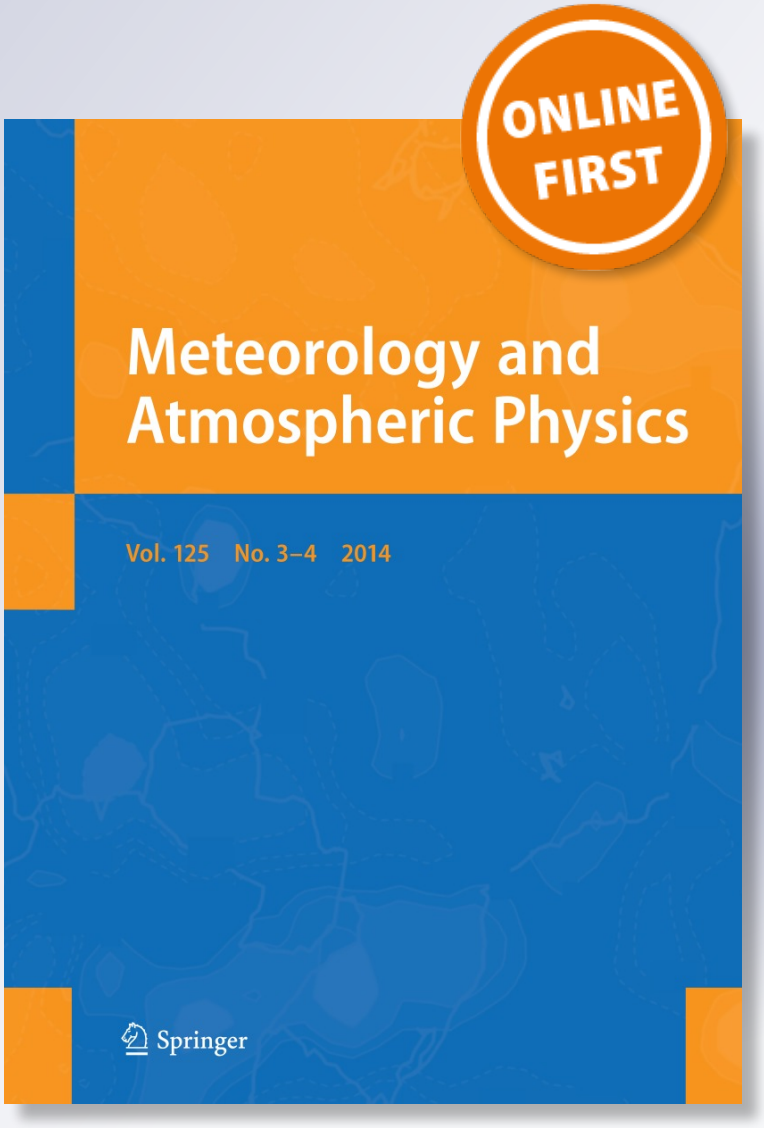


Springer

Meteorol Atmos Phys
DOI 10.1007/s00703-014-0342-4

ORIGINAL PAPER

# 4D tomographic reconstruction of the tropospheric wet refractivity using the concept of virtual reference station, case study: northwest of Iran

**Zohre Adavi · Masoud Mashhadi-Hossainali**

Received: 23 April 2014 / Accepted: 18 August 2014


**Abstract** Iran enjoys a variety of climatological conditions. Moreover, numerical weather prediction (NWP) models are not assimilated with the meteorological data in Iran, the country suffering from poor spatial and temporal resolution of radiosonde measurements. These facts make modeling of troposphere impossible using the measurements and NWP. On the other hand, the global positioning system (GPS) has been emerged as a valuable tool for modeling and remote sensing of Earth's atmosphere. This research is the first attempt to address the tropospheric wet refractivity modeling by GPS measurements in Iran. Changes of topography in the study area are taken into account. As a leading work, virtual reference stations (VRS) are used to fix the rank deficiency of the problem. The model space resolution matrix is used to achieve the optimum spatial resolution of the tomographic model and the optimum number of VRS stations. The accuracy of the developed model (KNTU1) is investigated by deploying radiosonde measurements.

## 1 Introduction

Water vapor is one of the most important weather parameters whose accurate measurement plays a significant role in weather prediction, upcoming storms, water resource management and reducing natural hazards (Bender and Raabe 2007; Brenot et al. 2014; Guerova 2003; Hoyle 2005; Lutz 2008; Manning et al. 2012). This parameter is one of the most variable components of the Earth's atmosphere. Its non-uniform distribution due to the atmospheric phenomena above the surface of the Earth depends on both space and time. Due to the limited spatial and temporal coverage of classic meteorological measurements, estimates of water vapor have been always contaminated by some uncertainties (Emardson et al. 1998; Jarlemark et al. 1998). On the other hand, the moisture affects the propagation of electromagnetic waves such as the global positioning system's (GPSs) signals. The spatial and temporal resolution of the GPS measurements is much higher than current systems used in meteorological researches. It has made the GPS a valuable tool for modeling and/or remote sensing of the earth's atmosphere.

Troposphere is the lower part of the atmosphere and practically defined as the neutral gaseous part from the surface to approximately 40 km above the earth. Here, propagation of electromagnetic waves is a function of the water vapor content, temperature and pressure. The refractivity index in this layer of atmosphere is empirically separated into the dry $(N_d)$ and wet $(N_W)$ components. The dry component is a function of temperature and pressure as well as the wet part affected by the water vapor and temperature (Langley 1998b; Schüler 2001; Spilker 1996d). Using surface meteorological measurements and the existing models such as the Saastamoinen's or Hopfield's, the dry part of the refractivity is normally modeled with an accuracy as large as a few millimeter (Bevis et al. 1992). Due to the high spatial and temporal variation of water vapor, precise modeling of $N_w$ is still the main challenge in modeling the tropospheric wet delay. Current

Responsible editor: M. Kaplan.

Z. Adavi (✉) · M. Mashhadi-Hossainali
Department of Geodesy and Geomatics Engineering, K. N.Toosi University of Technology, No. 1346, Vali_Asr Ave, Mirdamad Cr., Tehran, Iran
e-mail: zohre_adavi@yahoo.com; zohre_adavi@mail.kntu.ac.ir

M. Mashhadi-Hossainali
e-mail: masoud.hossainali@gmail.com; hossainali@kntu.ac.ir

Published online: 05 September 2014

developments in the GPS meteorology aim at solution of this problem as well as the other exiting challenges in this realm of research. Modeling the spatio-temporal variations of water vapor, estimating the integrated water vapor (IWV) and the precipitable water (PW) are some of examples for the developments mentioned above (de Haan and Barlag 2004; Vedel and Huang 2004).

In tomographic approach for modeling $N_w$, the Earth's atmosphere is divided into a finite number of three-dimensional elements (voxels). The GPS signals passing through each element are used for estimating this parameter. Due to the continuous motion of the GPS satellites, this method can be used for modeling a value parameter temporally and spatially. According to Menke (2012), the system of observation equation in the problem of tomography is a mixed-determined problem and the inversion may become singular because propagated signals do not pass through some of the model elements within the area of interest. To obtain a unique solution for this problem, several methods have been proposed. Hirahara (2000) has added horizontal and vertical constraints to the system of observation equations. Flores et al. (2000) have solved the tomographic problem using a Kalman filter. Nilsson and Gradinarsky (2006) found the solution directly through the GPS phase measurement equations. Algebraic reconstruction technique is also used for reconstructing a tomographic model (Bender et al. 2011). Rohm and Bosy (2011) proposed a set of parameters, which had been derived from the analysis of air flow to the corresponding system of equations. Radiosonde measurements and radio occultation profiles are two independent sets of constraints which has also been used to fix the rank deficiency of the problem (Bender et al. 2011; Foelsche and Kirchengast 2001; Xia et al. 2013).

This research is the first attempt for tomographic reconstruction of the wet refractivity in Iran. The concept of virtual reference station (VRS) has been used to find a unique solution for the problem. It has been shown that the appropriate distribution of virtual reference stations reduces the elements of the model null space to the trivial ones. In order to avoid over-constraining the problem, the number of these stations has been minimized.

The next section of this paper discusses on the tomographic reconstruction of the refractivity parameter, and the proposed model is investigated using the concept of resolution matrix. The adopted methodology to constrain the problem, i.e., deploying concept of VRS in tomographic reconstruction of the refractivity parameter, is also given. In the last section, the study area is introduced and also numerical results and the corresponding discussions are given. Reconstructed 4D model of this research has been verified using the radiosonde profiles of the study area.

## 2 Methodology

First, tomographic reconstruction problem of the wet refractivity is introduced. Then, concept of virtual reference station and its application is given. Using the resolution matrix, an optimum size of model elements is derived. Finally, the adopted method to compute a regularized solution is described.

### 2.1 Tomographic modeling

The slant total delay (STD) of the GPS signals in the troposphere is computed using the following equation (Bevis et al. 1992):

$$\mathrm{STD} = 10^{-6} \int_S N \, \mathrm{d}s \tag{1}$$

where $N$ is the refractivity parameter, and $S$ is the signal path between a satellite and a receiver. Using the wet and the dry components of refractivity, STD can be expressed in terms of the slant hydrostatic (SHD) and the slant wet delays (SWD) as given below:

$$\mathrm{STD} = \mathrm{SHD} + \mathrm{SWD} = 10^{-6} \int_S (N_\mathrm{d} + N_\mathrm{w}) \, \mathrm{d}s \tag{2}$$

The dry and wet components of the refractivity are computed by [See for e.g., (Kleijier 2004)]

$$N_\mathrm{d} = k_1 \frac{P_\mathrm{d}}{T} Z_\mathrm{d}^{-1} \tag{3}$$

$$N_\mathrm{w} = \left[ k_2' \frac{e}{T} + k_3 \frac{e}{T^2} \right] Z_\mathrm{w}^{-1} \tag{4}$$

Here, $k_1 = 77.59 \pm 0.08 \ \mathrm{KhPa}^{-1}$, $k_2' = 24 \pm 11 \ \mathrm{KhPa}^{-1}$, $k_3 = 3.75 \pm 0.03 \ (\times 10^5 \ \mathrm{K}^2\mathrm{hPa}^{-1})$ and parameters $T$, $P_\mathrm{d}$ and $e$ are temperatures, the partial pressure of dry gases and the water vapor of the atmosphere, respectively. $Z_\mathrm{d}$ and $Z_\mathrm{w}$ are known as the dry and the wet coefficients of compressibility. These coefficients are close to unity when the Earth's atmosphere is in a normal weather condition.

The slant hydrostatic and wet delays are computed from the corresponding parameters in the zenith direction using the dry and wet mapping functions:

$$\mathrm{STD} = m_\mathrm{d}(\mathrm{elv}) \, \mathrm{ZHD} + m_\mathrm{w}(\mathrm{elv}) \, \mathrm{ZWD} \tag{5}$$

elv is the elevation of the individual STD, ZHD and ZWD are the hydrostatic dry and wet delays in the zenith direction and, $m_\mathrm{d}$ and $m_\mathrm{w}$ are the corresponding mapping functions, respectively. It should be noted that this research deploys the GMF mapping function (Böhm et al. 2006).

Equation (2) is the mathematical model, which is used in tomographic reconstruction of the $N_\mathrm{w}$ parameter. For this purpose, the hydrostatic component should be subtracted

from the total slant delay. If precise surface meteorological parameters are known, ZHD can be computed by an accuracy of a few millimeters using, for example, Saastamoninen's model (Bevis et al. 1992; Davis et al. 1985). According to Saastamoinen (1973)

$$\mathrm{ZHD} = \frac{0.002277\, P_s}{(1 - 0.00266\, \cos(2\phi) - 0.00000028\, H)} \tag{6}$$

where $P_s$ is the surface pressure in millibar, $\phi$ and $H$ are the latitude and geodetic height in meters, respectively. The zenith total delay can be computed using GPS-processing software. To this end, the Bernese GPS software has been used (Dach et al. 2007). Hydrostatic zenith delays are then subtracted from the computed total delays in the zenith direction. Multiplying the wet mapping function to the obtained results, the slant wet tropospheric delays are derived. Computed slant wet delays (SWDs) are the required inputs for tomographic reconstruction of the wet refractivity as given by:

$$\mathrm{SWD} = 10^{-6} \int_S N_w \, \mathrm{d}s \tag{7}$$

This equation is derived as an ill-posed inverse problem, i.e., usually solutions are not unique and stable. In case of the GPS tomography, there is a necessity to deal with incomplete input data due to non-optimal spatial GPS slant coverage of the atmosphere for a tomographic reconstruction. The other reason is the wide spatial and temporal verity (Bender et al. 2009; Bender and Raabe 2007). In fact, some voxels are overdetermined while the others are underdetermined. Hence, the whole equation system is mixed-determined (Menke 2012) and the inversion may be singular.

The observation Eq (7) is made up for every receiver and all of the visible satellites in each measurement epoch. Therefore, Eq (7) has to be changed into a discrete form. For this purpose, troposphere should be divided into a finite series of elements. $N_w$ is assumed to be fixed in each element of this model. Since as the signal path $S$ is a function of the wet refractivity field, the observation Eq (7) is nonlinear too. This equation is linearized by assuming that the signal path is known, e.g., a straight line with small segments. In matrix notation, the discretized linear form of Eq (7) is written by the following form (Flores et al. 2000):

$$\mathbf{d} = \mathbf{A}\mathbf{m} \tag{8}$$

The $\mathbf{d}$ vector consists of the slant wet delays. $\mathbf{m}$ is the vector of unknown parameters ($N_w$ parameters) and $\mathbf{A}$ is the design matrix whose dimension is $m \times n$ where $m$ is the number of measurements, and $n$ is the number of the model elements. The parameter $m$ depends on the selected time resolution, the number of GPS stations and the number of visible satellites. The general form of this matrix is as follows (Rohm and Bosy 2009):

$$\mathbf{A} = \begin{bmatrix} d_{11} & d_{12} & d_{13} & d_{14} & \dots & d_{1m} \\ d_{21} & d_{22} & d_{23} & d_{24} & \dots & d_{2m} \\ \vdots & \vdots & \vdots & \vdots & \ddots & \vdots \\ d_{n1} & d_{n2} & d_{n3} & d_{n4} & \dots & d_{nm} \end{bmatrix} \tag{9}$$

where $d_{ij}$ is the length of $i$th ray, which passes through $j$th model element. Usually the refraction of rays is ignored (De Brito Mendes 1999). Therefore, assumed straight lines are used to model the propagation of electromagnetic waves.

The design or coefficient matrix $\mathbf{A}$ depends on the geometry of the model (size of voxels) as well as the geometry of the measurements (Bender et al. 2011). The model geometry is defined according to the size and the topography of the study area. Nevertheless, there are usually some limitations in this respect. For example, the vertical resolution of the model has to be selected 3–5 times smaller than the horizontal one (Bosy et al. 2010).

### 2.2 Constraining the problem using virtual reference stations

The VRS concept is referred to "observation" data for a non-existent, so-called virtual reference station, which is close to a rover receiver (Vollath et al. 2000). The virtual station data are not obtained from a real receiver, although it is computed through real GPS observations taken from the GPS reference stations. The virtual reference station data resembles what a real receiver would produce at the location of the virtual reference station as much as possible (Marel H-v-d 1998). The location of the VRS, i.e., the coordinates of the VRS, is usually taken as the approximate coordinates of the rover receiver. The concept of VRS is taken into consideration and is also more preferable in GPS RTK researches (Dai et al. 2001; Euler et al. 2001; Fotopoulos and Cannon 2001; Hu et al. 2002; Marel H-v-d 1998; Raquet and Lachapelle 2001; Rizos et al. 2000a; Vollath et al. 2000; Wanninger 1997; Wu 2009; Zhang et al. 2003). VRS observations are used to remove the distance-dependent errors in RTK positioning by forming double-differenced observations between the VRS and the user station (Erhu Wei et al. 2006; Rizos et al. 2000b; Wu 2009). The VRS observation data are generated in three steps (Odijk 2002; Wu 2009). At first, errors/corrections are computed for the GPS reference stations. Next, errors/corrections are computed at the position of the virtual station. Finally, the VRS observations are calculated using the errors/corrections of the previous step.

To reduce the error of atmospheric models used for producing VRS data, distance of GPS and VRS stations is

also constrained. The constraints depend on the meteorological conditions of the study area. For example, Zhang et al. (2009) suggested a maximum distance of about 50 km between a virtual and a GPS permanent station. Several methods have been proposed for finding the maximum distance, which assures negligible modeling error at the position of virtual stations. Ordinary kriging, low-order surface and linear interpolation are some of the methods [See for e.g., (Al-Shaery et al. 2011; Odijk 2002; Zhang et al. 2009)]. In this research, ordinary kriging is deployed. According to the obtained results, the interpolation of tropospheric error at the position of the GPS test stations is below $10^{-3}$ mm if the distances of VRS and GPS stations are less than 40–50 km in the study area of this research.

The tomographic model has zero projection onto the model null space, if each voxel includes at least one GPS station. Therefore, application of this idea to tomographic modeling of troposphere can repair the rank deficiency of this problem by constraining the model elements through which none of the GPS signals is passing. Obviously, the adopted number of VRS stations should be minimized since VRS data are contaminated by residual modeling errors. Moreover, overconstraining the problem with VRS stations significantly increases the redundancy of the problem. Consequently, the spatial distribution as well as the number of virtual stations depends on the geometry of the model and the distribution of the GPS stations in the study area.

### 2.3 Optimal geometry of the model

The concept of resolution is an efficient way to characterize the bias in a discrete inverse problem. Using this approach, it is possible to see how closely the inverse solution matches a given model, assuming that there are no errors in the data. Beginning with an arbitrary model $\mathbf{m}$, by multiplying $\mathbf{A}$ by $\mathbf{m}$, a corresponding data vector $\mathbf{d}$ can be found. Then, multiply generalized inverse of $\mathbf{A}\left(\mathbf{A}_{\dagger}\right)$ by $\mathbf{d}$, a least-squares solution $\left(\mathbf{m}_{\dagger}\right)$ is derived,

$$\mathbf{m}_{\dagger} = \mathbf{A}_{\dagger}\mathbf{A}\mathbf{m} \tag{10}$$

The model space resolution matrix, $\mathbf{R}_{\mathrm{m}}$ is then defined as,

$$\mathbf{R}_{\mathrm{m}} = \mathbf{A}_{\dagger}\mathbf{A} \tag{11a}$$

Using the theorem of singular value decomposition (Watkins 2002):

$$\mathbf{R}_{\mathrm{m}} = \mathbf{V}_p\,\mathbf{V}_p^T \tag{11b}$$

Here, $p$ is the number of singular values which are effectively non-zero, and the columns of the matrix $\mathbf{V}$ are the right singular vector of the coefficient matrix $\mathbf{A}$. If the model null space is trivial, $\mathbf{R}_{\mathrm{m}}$ is an identity matrix. But, if $\mathrm{rank}(\mathbf{A}) = p < n$ the model space resolution matrix is instead an asymmetric matrix describing how the inverse solution smears out the original model, $\mathbf{m}$, into a recovered model, $\mathbf{m}_{\dagger}$ (Aster et al. 2005). In other words, if any of the diagonal entries of this matrix are close to zero, then the corresponding model parameters will be poorly resolved.

The model space resolution matrix does not depend on a specific data value, but is an exclusively property of the matrix $\mathbf{A}$. Therefore, it reflects the experiment physics and geometry, and thus can be calculated during the design phase of an experiment to assess expected resolution for a model. An optimal design for the geometry of the model results in a resolution matrix, which is close to identity (Aster et al. 2005). Based on this idea, the concept of the model space resolution matrix is used to select the optimal geometry for the tomographic model. Since the horizontal and the vertical resolution of a tomographic model should also conform to the topography of the test area, to develop the tomographic model of this research, the topography of the study has also been taken into account.

### 2.4 Regularization method

Landweber is a well-known and a classic regularization technique. In this method, the following recursive equation is used for solving the ill-conditioned simultaneous system of equations $\mathbf{A}\mathbf{m} = \mathbf{d}$ (Aster et al. 2005; Bertero and Boccacci 1998; Elfving et al. 2010; Hansen 1998; Landweber 1951; Nikazad 2007):

$$\mathbf{m}^{k+1} = \mathbf{m}^k + \lambda_k\,\mathbf{A}^T(\mathbf{d} - \mathbf{A}\mathbf{m}^k) \tag{12}$$

The convergence of the above equations will be guaranteed if the parameter $\lambda_k$ is selected such that $0 < \lambda < 2/\sigma_{\max}^2$. Here, $\sigma_{\max}$ is the largest eigenvalue of matrix $\mathbf{A}$ (Aster et al. 2005). Nikazad (2007) reports on the application of this method as a tool for tomographic reconstruction of an image.

Like the other recursive regularization techniques, after a specified number of iterations, the approach approximates the solution closely while in additional iterations the small singular values of the matrix $\mathbf{A}$ amplifies the impact of the measurement noise on the solution. Consequently, the solution diverges to the one satisfying the least square constraints. This problem is known as the semi-convergence of solution in a recursive regulation technique (Rasmussen 2001).

The best way to obtain a solution for the semi-convergence problem is using get-at-able initial values of the solution. If no initial value is available, other methods such as the L-Curve method, discrepancy principal (DP), generalized cross validation (GCV) and flattest slope (FS) may be used (Golub and Matt 1997; Hansen 1998; Wu 2003).

$\lambda$ is obtained by different approaches. By optimal choice approach, the value of $\lambda_k$ is determined through searching in a range of $0 < \lambda < 2/\sigma^2_{\max}$ (Elfving et al. 2010). Optimal choice requires beforehand determination of the exact solution. Therefore, there is a necessity to train the algorithm using simulated data for real measurements (Elfving et al. 2010). Other techniques deployed to achieve $\lambda_k$ are $\psi_1$-based relaxation strategy, $\psi_2$-based relaxation strategy, line search and modified $\psi_1$ and $\psi_2$ strategies (Elfving et al. 2010).

In this paper, we used modified $\psi_2$ strategy. To reach optimum number of iterations required, the $N_w$ profile derived by the radiosonde data is used. Specifically, a vertical profile is extracted from the reconstructed image at the position of the radiosonde station at each iteration. This profile is compared to the $N_w$. The number of iterations, which RMSE of the reconstructed image is minimized in, has been selected as the optimum one.

### 2.5 Accuracy analysis

Regarding to any tomographic model, a key sector is the analysis of the accuracy and precision of the obtained results. RMS, bias and standard deviation (std) are normally used for this purpose (Rohm and Bosy 2009; Shangguan et al. 2013). These statistics are computed using the following equations (Guerova 2003):

$$\mathrm{RMSE} = \sqrt{\frac{1}{N}\sum_{i=1}^{N}\left(N^i_{\mathrm{wm}} - N^i_{\mathrm{wo}}\right)^2} \tag{13}$$

$$\mathrm{bias} = \frac{1}{N}\sum_{i=1}^{N}\left(N^i_{\mathrm{wm}} - N^i_{\mathrm{wo}}\right) \tag{14}$$

$$\mathrm{std} = \sqrt{\mathrm{RMSE}^2 - \mathrm{bias}^2} \tag{15}$$

Here, $N^i_{\mathrm{wm}}$ is the modeled wet refractivity in the $i$th voxel and $N^i_{\mathrm{wo}}$ is wet refractivity computed through a radiosonde profile. Moreover, $N$ is the number of the sample elements.

## 3 Numerical results and conclusions

Introducing the study area and the network of GPS stations used in this research, the adopted strategy to analyze the GPS measurements is discussed in detail. Next, using the concept of resolution matrix, the optimum size of the model and the optimum number of the required VRS stations to constrain the problem are analyzed. Finally, the reconstructed tomographic image is validated using the radiosonde data profiles.

### 3.1 Study area and the GPS network stations

Iran is a vast country that requires continuous monitoring of the weather due to various climates and different climatic phenomena such as heavy precipitations in the northern parts and huge tornadoes in southern regions. Climate variability in Iran is such that the annual precipitation in some southern cities of this country does not exceed 40 mm, while precipitation more than 600 mm has been reported in the western regions. Also, due to the lack of data and an organized data acquisition system, numerical models are not assimilated with regional data acquired in Iran. For example, the number of radiosonde stations, which are used to forecast the weather and climate changes, are only 14 which non-uniformly cover the country and are not launched regularly as well. Using the tomography method, these models can be improved. The permanent GPS stations as well as tomographic models can be used to establish a weather monitoring system in each region of the country, not only to improve the weather predictions, but also to increase the positioning accuracy.

In this research, the northwest part of the country has been selected due to its submontane topography, relatively dense permanent GPS stations and the existence of reasonable meteorological data in this area. National Cartographic Center (NCC) of Iran initiated the establishment of the Iranian Permanent GPS Network (IPGN) in December 2006. GPS stations are equipped with double frequency Ashtech UZ12 receivers, Chock ring antennas for mitigating the multipath effect, solar panels, power supply, tilt meters and the other standard equipments which are normally used in a permanent GPS station. Some of the GPS stations are also equipped with M3A meteorological sensors for measuring temperature (with the accuracy of $\pm 0.1^{\circ}$C), pressure (with the accuracy of $\pm 0.08$ hpa) and humidity (with the accuracy of $\pm 2\%$), IPGN initially consisted of 106 GPS stations. The northwestern part of the country, including the test area of this research, is covered by 15 stations. The distribution of the GPS stations, which are used in this study is shown in Fig. 1. Two IGS stations zeck and tehn, which are nearby to the study area are also added to the configuration of the GPS stations of this study mainly to address the reference frame issue for analyzing the GPS measurements (Becker et al. 2002). Carrier beat phases were measured in full wavelength and also sampling interval of the carrier beat phases is 30 s at all stations.

Since some of the GPS stations are equipped with meteorological sensors, 10 synoptic weather stations have been selected to obtain meteorological data where the other GPS stations are located. The only radiosonde station of this study is located in the vicinity of the Tabriz city (see

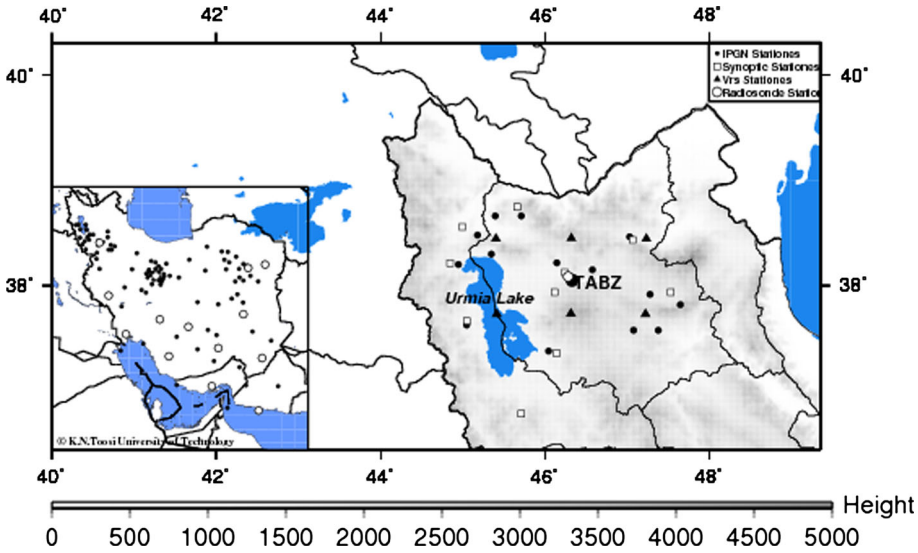


**Fig. 1** Distribution of the GPS stations on the background of topographic map in the study area of this research

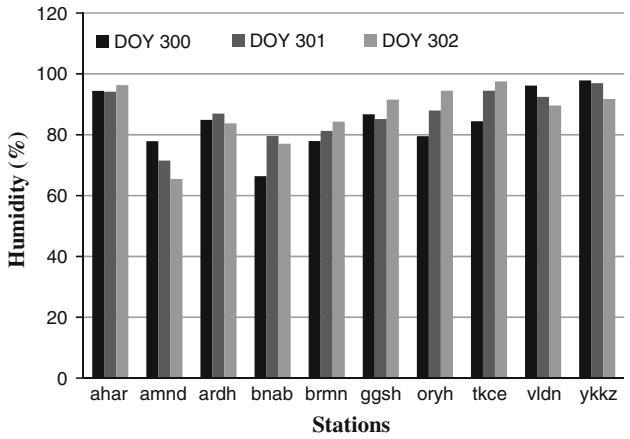


**Fig. 2** Relative humidity in some of the permanent GPS station of this research

Fig. 1). Dual frequency GPS measurements of DOYs[1] 300, 301, 302 in the year 2011 are used here. According to the meteorological reports during this time interval, the humidity of the study area is maximal.

Tomographic model of this study enjoys a temporal resolution of 1 h following the temporal resolution of the world reference forecasting (WRF), the available numerical weather prediction (NWP) model. The initial values required to solve observation equations are extracted from NWP model. Consequently, the reconstructed model consists of 72 epochs. Radiosonde balloons are launched once a day in the radiosonde station of Tabriz. Therefore, the accuracy of the developed model can be evaluated only at three successive epochs.

[1] Day Of Year.

The height of the GPS stations varies from 1,300 to 1,950 m above the mean seal level (MSL) of Iran. Figure 1 illustrates the height difference of the adopted GPS stations.

Meteorological data are recorded continuously and also available at the GPS stations equipped with meteorological sensors. Figure 2 reports on the humidity in these stations for the DOYs 300, 301 and 302.

### 3.2 GPS data processing

The Bernese GPS software version 5.2 was used to process the data. The GPS data-processing steps by this software are illustrated in the flow diagram of Fig. 3 (Dach et al. 2007). Providing a campaign, observation files were transferred from the RINEX (Receiver INdependentEXchange) ASCII format (Gurtner 1994) into the Bernese binary format. As a result, the code and phase zero difference header and observation files were produced. The IGS (International GPS Service for Geodynamics) antenna phase center offset and variation calibration table (Rothacher et al. 1996) is used to avoid the systematic effect of using different antenna types in the regional and the local stations. To get high precision results, CODE (Center of Orbit Determination in Europe) precise orbits and earth rotation parameters were used (Dach et al. 2007). Minimum elevation cut-off angle was set to 10° for processing the data in all epochs (Rothacher et al. 1998).

Carrier beat phases were preprocessed for detecting the cycle-slips and their repair in automatic mode using L3 frequency and L3 triple-difference solutions. Not only in the preprocessing of the data, but also in the final steps of parameters estimation and the computation of the combined solution, the input options were mostly considered as the default values that are recommended by the Bernese

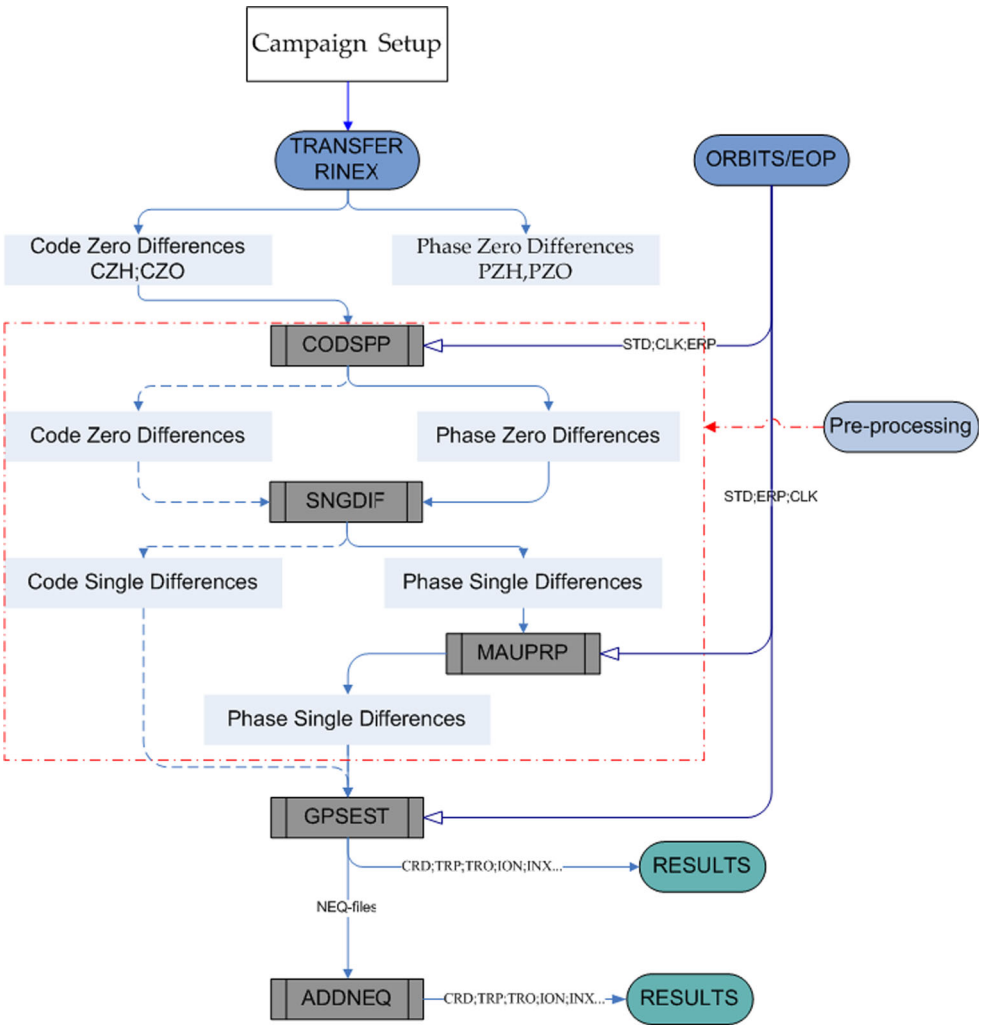


**Fig. 3** The flow diagram for processing the GPS data using the Bernese GPS data processing software

team. Short and long baselines are processed simultaneously. OBS-MAX strategy is used in order to find the best independent baselines from all possible. Observations whose residuals are larger than 0.003 m are considered as outliers and marked out in the observation files during the data-snooping process. Initial phase ambiguities are resolved using the QIF (Quasi Ionosphere Free) (Mervart 1995). Site-specific troposphere parameters are estimated at each station and on each day to compute the effect of troposphere error on ambiguities resolution. Generally, ZTD parameters were estimated with 1-h time interval at each of the GPS stations. For long baselines (baselines longer than 10 km), the IGS GIM models (Schaer 1999) that are estimated with the same dataset are used to improve the ambiguity resolution. This was done to mitigate ionospheric error. The consistency of the resolved integer ambiguities with the software implemented mathematical models is also investigated through evaluating the a posteriori variance of unit weight in the float solution (obtained from the first run of the program GPSEST in which the ambiguities are treated as unknown parameters) and the fixed solution (obtained in the third run of this program, in which the resolved integer L1 and L2 ambiguities are introduced as known parameters to the system of normal equations). A consistent integer ambiguity results in a smooth change in the a-posterior variance of unit weight, whereas an inconsistent one can produce abrupt variations in the parameter estimation.

### 3.3 Tomographic model

The vertical resolution of the tomographic model is 500 m and extended from the surface to the height of 4 km and then is reduced to 1,000 m. The model is extended to the height of 10 km from the surface of the Earth.

The horizontal resolution of the NWP model is the first suggestion for the horizontal resolution of the tomographic model, while this value is 10 km for the WRF model. The spatial distribution of GPS stations in this study is inadequate for such a high horizontal resolution,

since the rank deficiency of the corresponding model would be 2,790. Consequently, to achieve a unique solution of the problem, the simultaneous system of observation Eq (8) must be tightly constrained. Since the number of required constraints is very large, the corresponding solution shall be governed more by the constraints rather than the GPS measurements. This fact is also valid when the horizontal resolution of the model is reduced to 20 km. For a better visualization, Fig. 4 illustrates the model resolution matrix in small bands, the spatial distribution of the GPS stations and the horizontal resolution of the tomographic model which is 20 km. The model space resolution matrix illustrates that many of the model parameters will be resolved poorly if this resolution is selected for the model.

To find an appropriate horizontal resolution for the model, the model space resolution matrix is computed for tomographic models whose voxel sizes are 30, 40 and 50 km, respectively. Figure 5 illustrates the obtained results. According to the obtained results, the horizontal resolution of 50 km is superior to the others since the number of model parameters that are resolved poorly decreases further in comparison to the others. Specifically, 18 % of the model parameters are resolved poorly when the horizontal resolution of the model is 30 km. This value is decreased to 9 and 2 % for the horizontal resolutions of 40 and 50 km, respectively.

**Fig. 5** The 3D tomographic model and the model space resolution matrices plotted only on diagonal form that elements 1 or close to 1 (illustrated in small bands for a better visualization) for the horizontal resolutions of (**a**) 30 km, (**b**) 40 km and (**c**) 50 km. Shaded voxels in 3D tomographic models illustrate the position of the model elements which are poorly resolved ▶

Here, the simultaneous system of observation equations is constrained by virtual stations. To reduce atmospheric modeling errors, the distance of a VRS to at least two nearby GPS station should be less than 50 km which is possible when the horizontal resolution of the model is 40 km. The distribution of virtual stations should be such that the rank deficiency of the coefficient matrix **A** in Eq (8) is fixed by the minimum number of VRS stations. Otherwise, reconstructed image of the wet refractivity shall be contaminated by the residual model errors, which are inherent in the VRS measurements. Here, the method of trial and error is used to determine the minimal number of VRS stations. According to the obtained results, at least six virtual reference stations are needed to repair the rank deficiency of the problem. Figure 6 illustrates the first horizontal layer of the model and also the distribution of the GPS and VRS stations. Figure 5b-1 provides a 3D

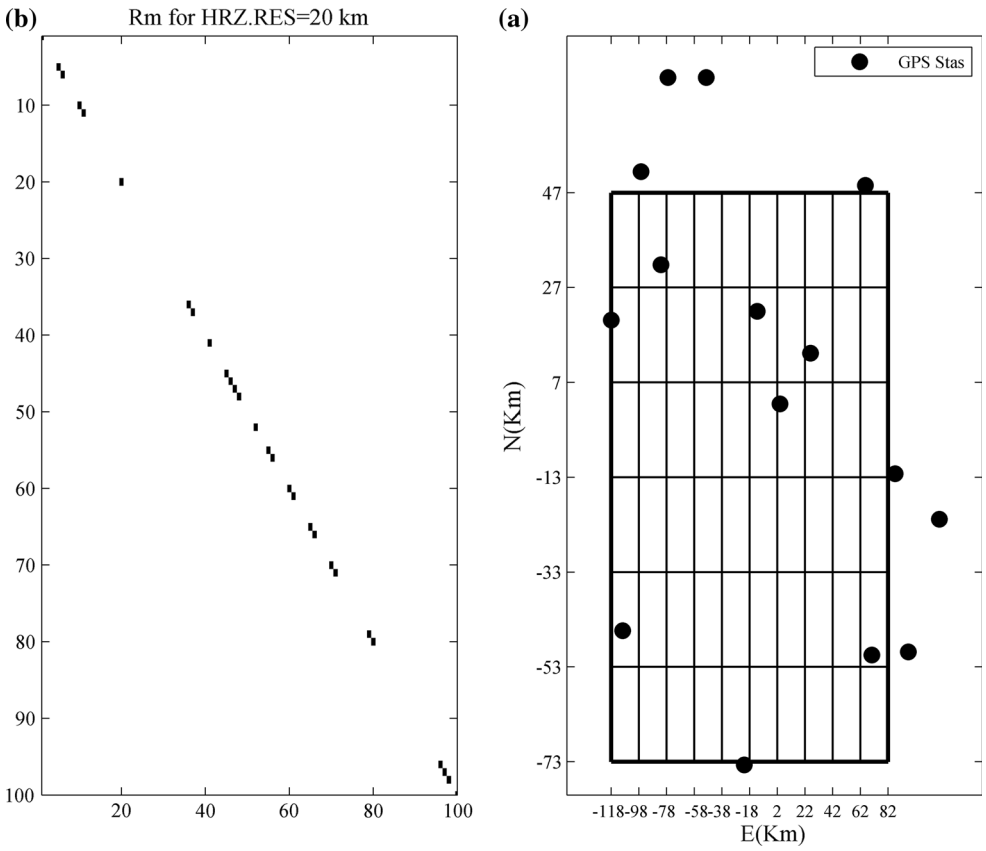


**Fig. 4** (**a**) The model space resolution matrix plotted only on diagonal form, and (**b**) the distribution of GPS stations with respect to a tomographic model whose horizontal resolution is 20 km. The *rectangle* illustrates the boundary of study area

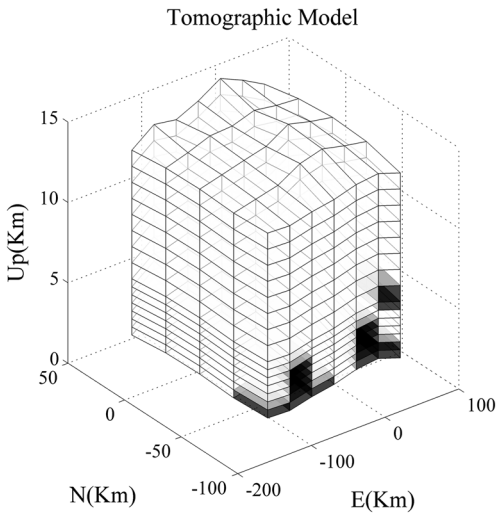


(a-1)

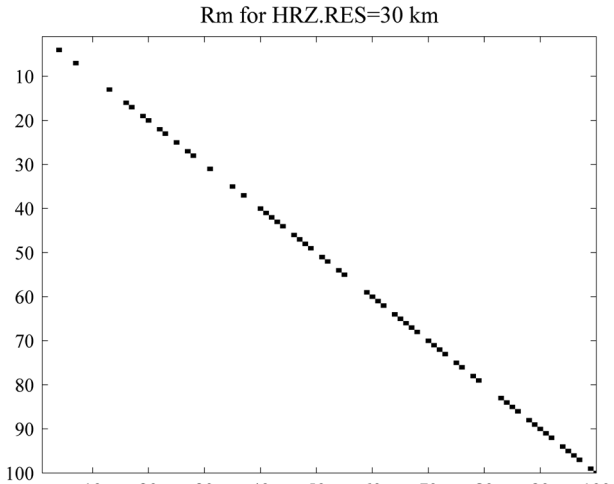


(a-2)

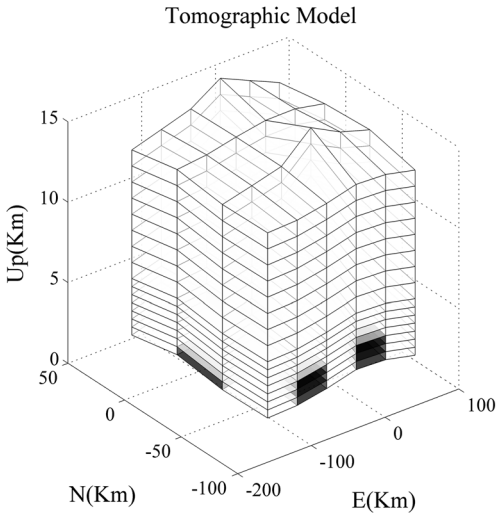


(b-1)

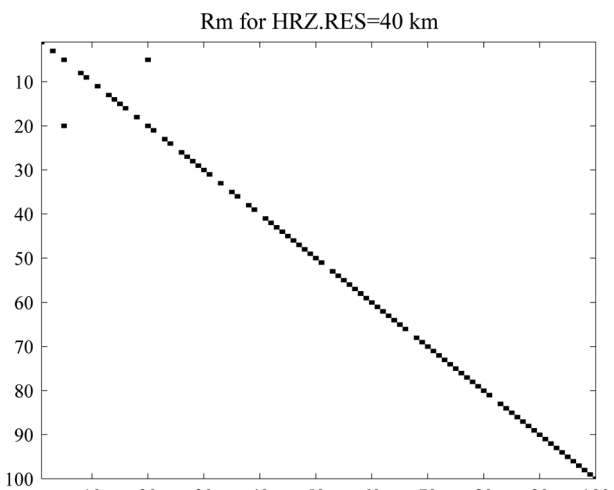


(b-2)

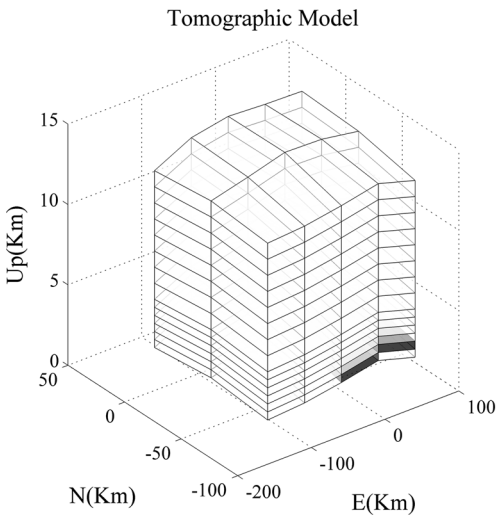


(c-1)

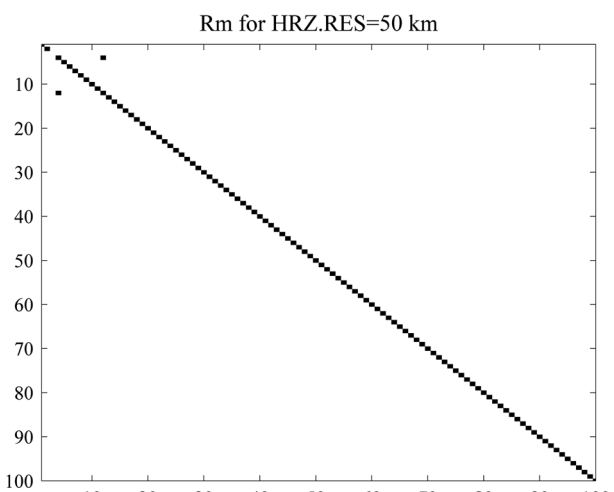


(c-2)

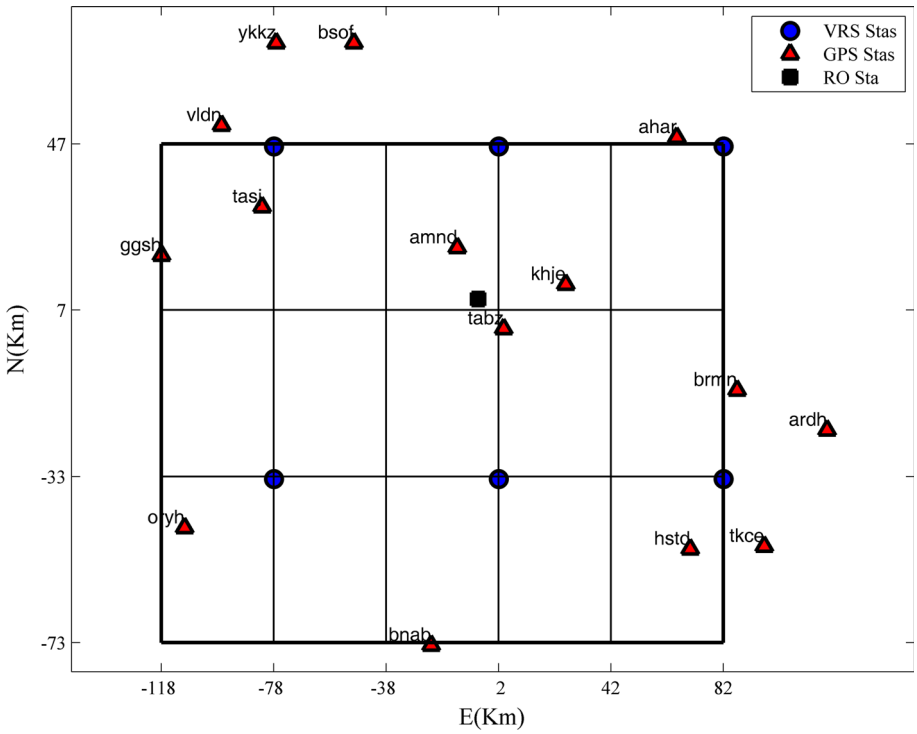


**Fig. 6** The spatial distribution of the GPS and VRS stations in first horizontal layer of the tomographic model within the test area of this study. The *rectangle* illustrates the territory of the study area

perspective of this model in the ENU coordinates (Cai et al. 2011; Grewal et al. 2007). According to this figure, the tomographic model of this study considers the topography of the study area as well. Applying the virtual stations improves the resolution of the model. This is shown in Fig. 7 by comparing the resolution matrices of the tomographic model before and after deploying theVRS constraints.

### 3.4 Reconstructed image and its accuracy analysis

Using previous discussed method, a 4D tomographic image has been reconstructed for the wet refractivity in the study area of this research. In order to analyze the efficiency of the proposed method, the $N_w$ profile which is reconstructed at the position of the Tabriz radiosonde station ($U_{\text{Tabriz}} = 1835$ m) has been compared to the corresponding profile, which is obtained from the radiosonde data (Shangguan et al. 2013, 2011). Tabriz radiosonde station is the only radiosonde station within the study area of this research. Therefore, it is not possible to check the accuracy of the developed model in the other parts of this area. This analysis has been done for three epochs. Figure 8 demonstrates the corresponding results and Table 1 reports on the corresponding details. Equations (13), (14) and (15) have been used for this purpose. Heights of the voxels' center are used to illustrate reconstructed images and the smoothed radiosonde profiles.

According to Shangguan et al. (2013), the discrepancy between radiosonde observations and the tomographic model can be due to a true error in the tomography, which can be attributed to either few slants in the developed model or instability of solution, real difference in atmospheric conditions which are sampled at different locations and times and finally true errors in the radiosonde estimates of the wet refractivity. The model space resolution matrix provides an insight into the minimum number of required slants in the tomographic model of this research. Nevertheless, it is not possible to distinguish the individual contribution of the other sources in the reported bias. But, a priori information of the measurement process can help understand whether the estimated bias is also contaminated by true errors in radiosonde estimates. According to Iran's Meteorological Organization (IRIMO), the radiosonde temperature and humidity sensors are calibrated before launching a radiosonde balloon. This is known as the ground check. Improper calibration of the sensors results in a systematic error in the outputs. The corresponding bias decreases as the height of the sensors increases. Such a bias has been committed in the Tabriz radiosonde station at DOY 301 and DOY 302. Nevertheless, the ground check process has been perfectly done at DOY 300. Therefore, the existing discrepancy between the estimated biases (See Table 1) in DOYs 301 and 302 should be partially assigned to the true errors in radiosonde results.

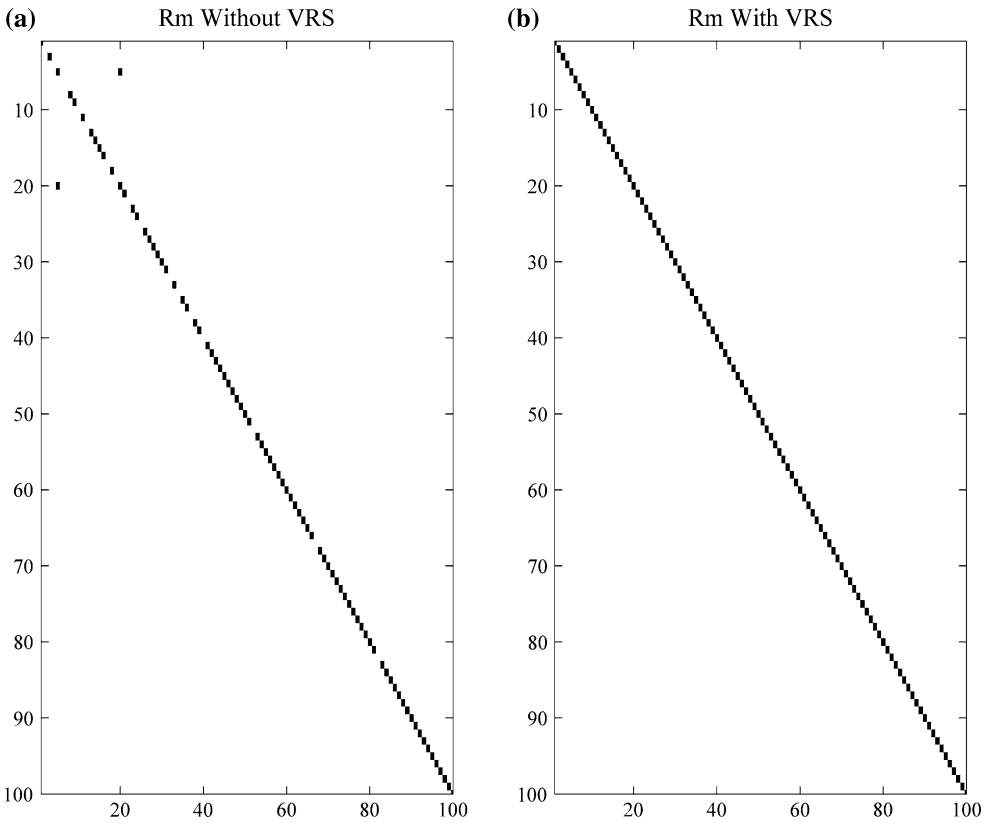


**Fig. 7** Resolution matrices plotted on diagonal form (illustrated in small bands for a better visualization) for the tomographic model of this research before (**a**) and after (**b**) the application of VRS constraints

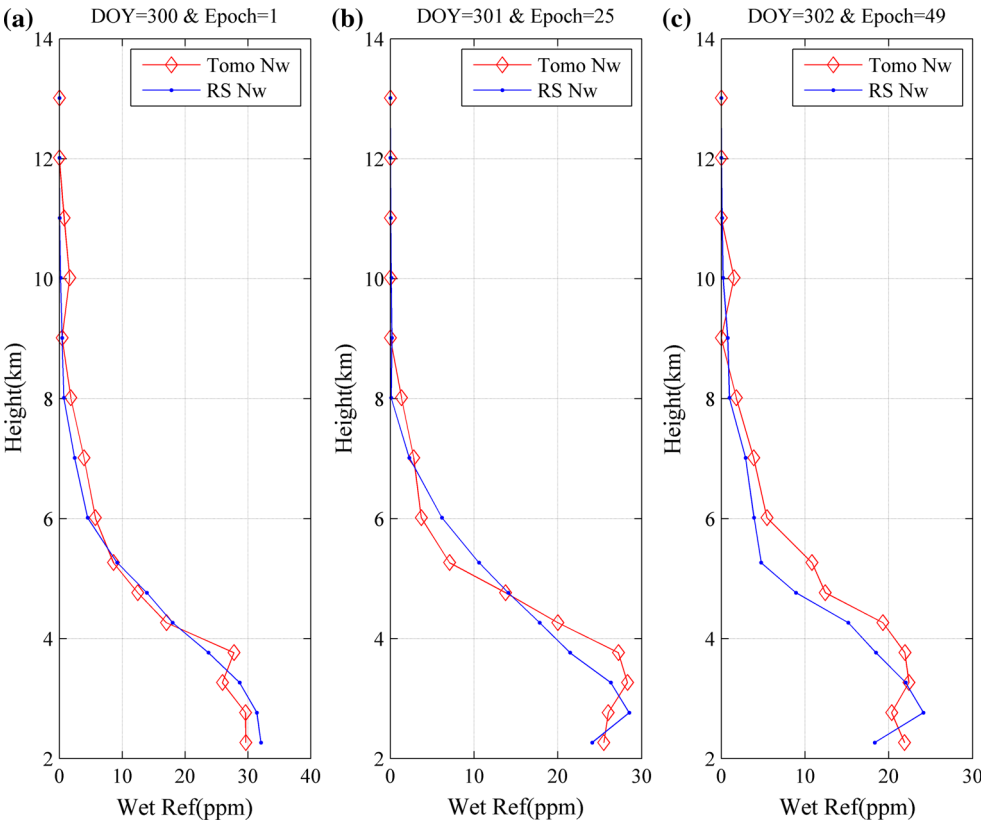


**Fig. 8** The comparison of tomographic profiles to the profile derived from radiosonde data: the 1st epoch (**a**), the 25th epoch (**b**) and the 49th epoch (00 $^{h}$:00 $^{m}$ in UTC) (**c**)

**Table 1** RMSE, bias and std for three epochs 1, 25 and 49

| Day | RMSE (ppm) | Std (ppm) | Bias (ppm) |
|---|---|---|---|
| DOY 300 | 1.72 | 1.72 | 0.0045 |
| DOY 301 | 2.17 | 2.15 | 0.26 |
| DOY 302 | 2.72 | 2.34 | 1.40 |

## 4 Concluding remarks

This study is the first attempt to address the tomographic reconstruction problem of the wet refractivity in Iran. The northwestern part of the country has been considered as the study area in this research due to submontane topography, relatively dense GPS network and the existence of reasonable meteorological data in this area. Virtual reference stations have been used for computing a unique solution of the problem. The distribution of VRS stations as well as the horizontal resolution of the model has been selected using the concept of model space resolution matrix. To avoid over-constraining the problem, the minimal number of virtual stations is used. The accuracy of the developed model has been analyzed using the only radiosonde station within the study area of this research. Using virtual stations, tomographic modeling appears to be plausible where the GPS station network is not dense and the residual modeling errors at the VRS stations are small.

**Acknowledgments** During this research, Mr. Akbar who is a member of the meteorological organization of Iran, kindly provided us valuable remarks. His cooperation is appreciated here. The meteorological organization of Iran provided the radiosonde profiles with dense pressure levels of the Tabriz station and the observation files of Synoptic stations in the northwestern part of the country for this research. This collaboration is also appreciated here. We are grateful to the National Cartographic Center (NCC) of Iran for providing the observation files of the Azerbaijan sub-network of the Iranian Permanent GPS Network too.

## References

Al-Shaery A, Lim S, Rizos C (2011) Investigation of different interpolation models used in network-RTK for the virtual reference station technique. J Glob Position Syst 10:136–148. doi:10.5081/jgps.10.2.136

Aster R, Borchers B, Thurber C (2005) Parameter estimation and inverse problems, vol 90. Elsevier Academic Press, USA

Becker M, Bruyninx C, Fernandez R (2002) Processing and Submission Guidelines for GPS Solutions to be Integrated to a WEGENER Data Base,Proceedings of WEGENER 2002. Athens, Greece, University of Athens, Jun 12-14

Bender M, Raabe A (2007) Preconditions to ground based GPS water vapour tomography. Ann Geophys 25(8):1727–1734

Bender M et al (2009) Estimates of the information provided by GPS slant data observed in Germany regarding tomographic applications. J Geophys Res. doi:10.1029/2008JD011008

Bender M et al (2011) Development of a GNSS water vapour tomography system using algebraic reconstruction techniques. Adv Space Res 47:1704–1720. doi:10.1016/j.asr.2010.05.034

Bertero M, Boccacci P (1998) Introduction to inverse problem in imaging. Institute of Physics, London

Bevis M, Businger S, Herring T, Rocken C, RA A, Ware RH (1992) GPS meteorology: remote sensing of atmospheric water vapor using the global positioning system. J Geophys Res 97(D14): 15787–15801

Böhm J, Niell A, Tregoning P, Schuh H (2006) Global mapping function (GMF): a new empirical mapping function based on numerical weather model data. Geophys Res Lett. doi:10.1029/2005GL02554

Bosy J, Rohm W, Sierny J (2010) The concept of the near real time atmosphere model based on the GNSS and the meteorological data from the ASG-EUPOS reference stations. Acta Geodyn Geomater 7:253–261

Brenot H et al (2014) A GPS network for tropospheric tomography in the framework of the Mediterranean hydrometeorological observatory Cévennes-Vivarais (southeastern France). Atmos Meas Tech 7:553–578. doi:10.5194/amt-7-553-2014

Cai G, Chen BM, Lee TH (2011) Unmanned rotorcraft systems. Springer, New York

Dach R, Hugentobler U, Fridez P, Meindl M (2007) Bernese GPS Software Version 5.0. Astronomical Institute, University of Bern, Bern

Dai L, Han S, Wang J, Rizos C (2001) A study of GPS/GLONASS multiple reference station techniques for precise real-time carrier phase–based positioning. In: 14th Internationl Technical Meeting of the Satellite Division of the US Institute of Navigation, Salt Lake City, Utah, 11–14 September, pp 392–403

Davis JL, Herring TA, Shapiro II, Rogers EE, Elgered G (1985) Geodesy by radio interferometry: effects of atmospheric modeling errors onestimates of baseline length. Radio Sci 20(6):1593–1607

De Brito Mendes V (1999) Modeling the neutral-atmosphere propagation delayin radiometric space techniques. University of New Brunswick, Fredericton

Elfving T, Nikazad T, Hansen PC (2010) Semi-convergence and relaxation parameters for a class of sirt algorithms. Electron Trans Numer Anal 37:321–336

Emardson TR, Elgered G, Johansson JM (1998) Three months of continuous monitoring of atmospheric water vapor with a network of Global Positioning System receivers. J Geophys Res 103:1807–1820

Erhu Wei E, Chai H, An Z (2006) VRS virtual observations generation algorithm. J Global Position Syst 1–2:76–81

Euler HJ, Keenan CR, Zebhauser BE, Wübbena G (2001) Study of a simplified approach in utilizing information from permanent reference station arrays. Paper presented at the Proceedings 14th International Technical Meeting of the Satellite Division of the Institute of Navigation, Salt Lake City, USA, ION GPS-2001, September 11–14

Flores A, Ruffini G, Rius A (2000) 4D tropospheric tomography using gps slant wet delays. Ann Geophys 18(2):223–234. doi:10.1007/s00585-000-0223-7

Foelsche U, Kirchengast G (2001) Tropospheric water vapor imaging by combination of ground-based and space born GNSS sounding data. J Geophys Res 106(D21):27221–27231

Fotopoulos G, Cannon ME (2001) An overview of multi-reference station methods for Cm-level positioning. GPS solutions 4:1–10

Golub GH, Matt U (1997) Generalized cross-validation for large scale problems. J Comput Graph Stat 6(1):1–34. doi:10.1080/10618600.1997.10474725

Grewal MS, Weill RL, Andrews AP (2007) Global positioning systems, inertial navigation, and integration. Wiley, New York

Guerova G (2003) Application of GPS derived water vapour for numerical weather prediction in Switzerland. University of Bern, Bern

Gurtner W (1994) RINEX: The reciever-independent exchange format GPS World, Las Cruces: 48–52

Hansen PC (1998) Rank-deficient and discrete ILL-posed problems: numerical aspect of linear inversion, Philadelphia

Hirahara K (2000) Local GPS tropospheric tomography. Earth planet space 52(11):935–939

Hoyle VA (2005) Data assimilation for 4-D wet refractivity modelling in a regional GPS network. Calgary, Alberta

Hu GR, Khoo VHS, Goh PC, Law CL (2002) Internet-based GPS VRS RTK positioning with a multiple reference station network. J Global Position Syst 1:113–120

Jarlemark POJ, Johansson JM, Emardson TR (1998) Wet delay variability calculated from radiometric measurements and its role in space geodetic parameter estimation. Radio Sci 33:719–730

Kleijier F (2004) Troposphere modeling and filtering for precise GPS leveling. Delft, The Netherlands

Landweber L (1951) An iteration formula for Fredholm integral equations of the first kind. Am J Math 73:615–624

Langley R (1998b) Propagation of the GPS Signals, Chap 3, In: Teunissen, Kleusberg, pp 111–149

Lutz SM (2008) High-resolution GPS tomography in view of hydrological hazard assessment. ETH Zurich, Switzerland

Manning T, Zhang K, Rohm W, Choy S, Hurter F (2012) Detecting severe weather using GPS tomography: an australian case study. J Global Position Syst 11:58–70. doi:10.5081/jgps.11.1.58

Marel H-v-d (1998) Virtual GPS reference stations in the Netherlands. In: Paper presented at the Proc 11th International Technical Meeting of the Satellite Division of the US Institute of Navigation, ION GPS-98, Nashville, TN, September 15–18

Menke W (2012) Geophysical data analysis: discrete inverse theory MATLAB Edition. doi:10.1016/B978-0-12-397160-9.00001-1

Mervart L (1995) Ambiguity resolution techniques in geodetic and geodynamic applications of global positioning system. University of Bern, Bern

Nikazad T (2007) The use of land weber algorithm in image reconstruction. Linköpings University, Linköpings

Nilsson T, Gradinarsky L (2006) Water vapor tomography using GPS phase observations: simulation results. IEEE Trans Geosci Remote Sens 44:2927–2941

Odijk D (2002) Fast precise GPS positioning in the presence of ionospheric delays. University of Delft, The Netherlands

Raquet J, Lachapelle G (2001) Efficient precision positioning: RTK positioning with multiple reference stations. GPS World 12(48):53

Rasmussen JM (2001) Compact linear operators and Krylov subspace methods. Technical University Denmark, Denmark

Rizos C, Han S, Chen HY (2000a) Regional-Scale multiple reference stations for carrier phase-based GPS positioning a correction generation algorithm Earth. Planet Space 52(10):795–800

Rizos C, Han S, Chen HY (2000b) Regional-scale multiple reference stations for carrier phase-based GPS positioning a correction generation algorithm Earth. Planet Space 52:795–800

Rohm W, Bosy J (2009) Local tomography troposphere model over mountains area. Atmos Res 93(4):777–783. doi:10.1016/j.atmosres.2009.03.013

Rohm W, Bosy J (2011) The verification of GNSS tropospheric tomography model in a mountainous area. Adv Space Res 47:1721–1730. doi:10.1016/j.asr.2010.04.017

Rothacher M, Schaer S, Beutler G, Schlüter W, Hase HO (1996) Phase center variations of GPS antennas derived from GPS observations of specially designed calibration campaigns supplement to EOS, American Geophysical Union, 1996 Springer Meeting, May 20–24 77:G11A-16

Rothacher M, Springer TA, Schaer S, Beutler G (1998) Processing strategies for regional GPS networks. In: Brunner Fk (ed) International Association of Geodesy Symposia, vol 118. Advances in Positioning and Reference Frames, Springer, Berlin Heidelberg, pp 93–100. doi:10.1007/978-3-662-03714-0_14

Saastamoinen J (1973) Contributions to the theory of atmospheric refraction. Part II: refraction corrections in satellite geodesy. Bull Geod 107:13–34

Schaer S (1999) Mapping and predicting the earth's Ionosphere using the global positioning system. University of Bern, Bern

Schüler T (2001) On ground-based GPS tropospheric delay estimation

Shangguan M, Bender M, Wickert J, Raabe A (2011) Validation of GNSS water vapour tomography with radiosonde data. In: Geodätische Woche Nürnberg

Shangguan M, Bender M, Ramatschi M, Dick G, Wickert J, Raabe A, Gales R (2013) GPS tomography: validation of reconstructed 3-D humidity fiDiescludsssions with radiosonde profiles. Ann Geophys 31:1491–1505

Spilker J (1996d) Tropospheric Effects on GPS. In: Parkinson Spilker (eds) 1,Chap.13:517-546

Vedel H, Huang XY (2004) Impact of ground based GPS data on numerical weather prediction. J Meteorol Soc Jpn 82(1B):459–472

Vollath U, Buecherl A, Landau H, Pagels C, Wager B (2000) Multi-base RTK positioning using virtual reference stations.In: Paper presented at the Proceedings 13th International Technical Meeting of the Satellite Division of the US Institute of Navigation, ION GPS-2000, Salt Lake City, September, 19–22

Wanninger L (1997) Real-time differential GPS-error modeling in regional reference station networks. Paper presented at the Proceedings of the IAG scientific assembly, Rio de Janeiro, Sep

Watkins DS (2002) Fundamentals of matrix computations. Wiley, USA

Wu L (2003) A parameter choice method for Tikhonov regularization ENTA Kent State University 6:22

Wu S (2009) Performance of regional atmospheric error models for NRTK in GPSnet and the implementation of a NRTK system. RMIT University, Australia

Xia P, Cai C, Liu Z (2013) GNSS troposphere tomography based on two-step reconstructions using GPS observations and COSMIC profiles. Annales Geophysicae 31:1805–1815. doi:10.5194/angeo-31-1805-2013

de Haan S, Barlag S, Klein Baltink H, Debie F, van der Marel H (2004) Synergetic use of GPS water vapor and Meteosat images for synoptic weather forecasting. J Appl Meteorol 43:514–518

Zhang K, Roberts C Network-based real-time kinematic positioning system: current development in Australia. In: Geoinformatics and Surveying Conference, Malaysia, 7 Apr 2003

Zhang S, Lim S, Rizos C, Guo J Atmospheric decomposition for VRS based network-RTK system. In: 22nd International Technical Meeting of the Satellite Division of the US, Institution of Navigation, Savannah, Georgia, 22–25 September 2009, pp 2707–2716